Dynamic Article Links ▶

PAPER

Resistivity transition mechanism of silver salts in the next generation conductive ink for a roll-to-roll printed film with a silver network†

Dong-Youn Shin,[a] Minhwan Jung[b] and Sangki Chun*[b]

As the small size display market rapidly expands with the advent of smart phones and tablets, the industrial demand for a low cost transparent conductive film instead of an ITO sputtered one has expedited the development of a roll-to-roll printed one with a low temperature processable and highly conductive ink. The conventional conductive ink based on metallic nanoparticles capped with a polymeric dispersant, however, has difficulties in achieving high conductivity at a low curing temperature due to the unwanted residue of a polymeric dispersant. Therefore, a new kind of conductive ink was developed, where a silver salt replaces the role of a polymeric dispersant and also enriches the overall metallic content. The key to this new generation of conductive ink leans on the selection of a low temperature processable silver salt and the selection process of silver salts was on the basis of their thermogravimetric thermograms with the common belief that the thermogravimetric thermogram of a silver salt is coupled with its resistivity transition and final resistivity. In contrast to this common belief, our results show that the thermogravimetric behaviours of silver salts have little influence on their resistivity transition and final resistivity. With our comprehensive studies using various isomeric silver salts, we here suggest that the more persuasive and leading factors in determining the resistivity transition behaviour of a silver salt are stack integrity, phase transition, and the exothermic band in the differential scanning calorimetric thermogram. The next generation conductive ink with the most suitable silver salt was gravure-offset printed on a transparent and flexible film. Its sheet resistance after being cured at 150 °C is as low as 1 Ω □$^{-1}$ with the line width of 20 μm and the optical transmittance of 85% and above.

1. Introduction

Printed electronics based on printing technologies have been comprehensively investigated for years because of the great advantage they offer over conventional photolithographic processes. Printing technologies have the inherent characteristic of selectively depositing precious materials only where they are required, and numerous promising results have been achieved so far. The fabrication of active electronic components such as organic[1–5] and inorganic[6,7] thin film transistors, and passive electronic components such as capacitors,[8] RC filter circuits,[9] and antennas,[10] has been successfully demonstrated.

It is noteworthy that among many kinds of potentially printable devices, the industrial demand for a flexible and transparent conductive film rapidly increases *in lieu* of an ITO sputtered one

as the small size display market explosively grows with the advent of smart phones and tablets. As shown in Fig. 1, a highly transparent and conductive film is now continuously producible with a gravure-offset printing technology and the very key issue is the development of a highly conductive ink at a low curing temperature because of the use of polymeric substrates,[11,12] whose glass transition temperature is generally as low as approximately 150 to 200 °C such as polyethylene naphthalate (PEN) and cyclic olefin copolymer (COC).[13]

Here, low temperature processable conductive ink can be categorized into three generations. The first generation of conductive ink has been the solution form of organometallic compounds, which are finally reduced to elements such as gold,[14,15] copper[16,17] and silver[18–20] by thermal decomposition. Although the employment of organometallic compounds has unique features such as a relatively low thermal decomposition temperature around 150 °C and an enhanced degree of curing due to the absence of surfactants,[19] the metallic solid content is generally restricted by both the solubility of the organometallic compound in a solvent and the molecular fraction of the metal in the compound itself.

Therefore, a suspension form of metallic nanoparticles as the second generation conductive ink has been exploited to not only

[a]Department of Graphic Arts Information Engineering, Pukyong National University, San 100, Yongdang-dong, Nam-gu, Busan, 607-739, Republic of Korea
[b]Information and Electronic Materials Institute, LG Chem Research Park, 104-1, Moonji-dong, Yuseong-gu, Daejeon, 305-380, Republic of Korea. E-mail: sangki@lgchem.com
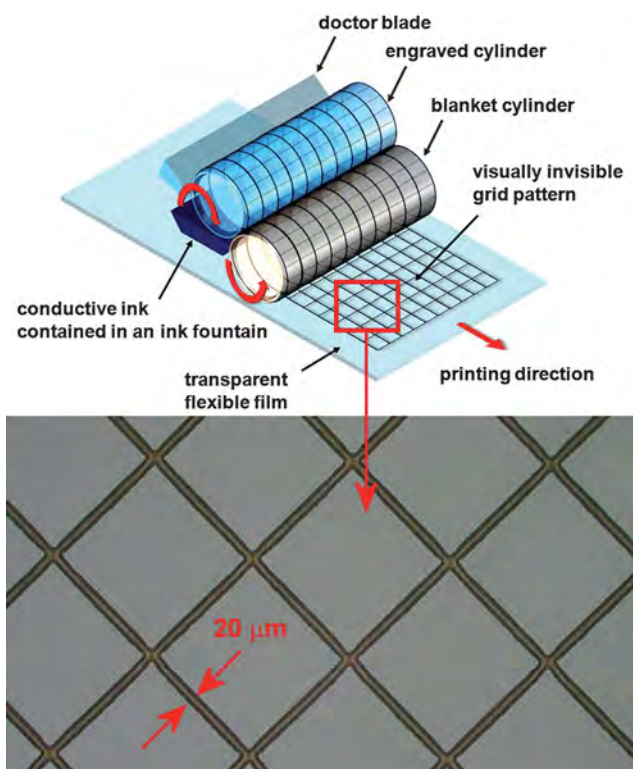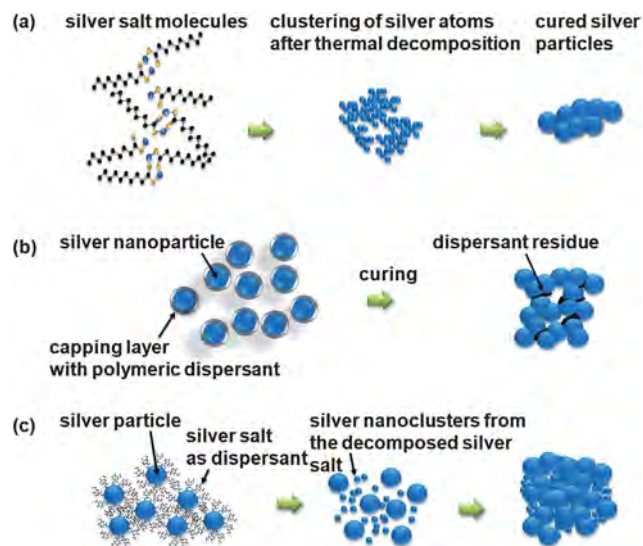
Fig. 1 Roll-to-roll printed transparent conductive film with a gravure-offset printing technology, where the line width is as narrow as 20 μm.

Fig. 2 Classification of conductive ink, (a) the first generation silver salt based ink, (b) the second generation nanoparticle based ink with a polymeric dispersant, and (c) the next generation conductive ink with metal particles and a silver salt as both a metallic additive and a dispersant.

enrich the metallic solid content of ink[21,22] but also lower the curing temperature because the employment of nanoparticles is known to induce a decrease of the melting temperature.[23,24] With metal nanoparticulate ink, various printing methods have been explored, such as inkjet printing,[25–29] screen printing,[30] and gravure printing.[31] The hybridization of multiple processes has also been attempted, such as micromolding and microtransfer,[32] inkjet printing and laser curing,[33] hot embossing and inkjet printing,[34] and surface energy patterning and spray coating,[35] to overcome the demerits of a single specific printing method.

However, the use of a surfactant to disperse metal nanoparticles in ink by encapsulating them tends to leave unwanted surfactant residues, which increase the overall resistivity of a cured metallic part. Because a higher curing temperature than the melting temperature of nanoparticles is required to remove such surfactant residues, the very benefit of using metal nanoparticles to decrease the curing temperature is impaired.

Therefore, the next generation of conductive ink was developed for a roll-to-roll printed transparent conductive film, where a silver salt is mixed with metal particulate ink not only to increase the overall metallic solid content of the ink but also to substitute a conventional polymeric dispersant, as shown in Fig. 2. The use of a silver salt as both a metallic additive and a dispersant in this next generation conductive ink leads to two main advantages. If the concentration of metallic particles is above a certain limit, the resulting viscosity of ink exponentially escalates in accordance with the Krieger–Dougherty model.[36,37] Therefore, the further enrichment of the metallic solid content of the ink should be done without any significant alteration of its viscosity since each printing technology has its own printable viscosity range.[38] This can be accomplished with a silver salt as a metallic additive.[31,39] Another advantage to the use of a silver salt *in lieu* of a polymeric dispersant is the reduction of resistivity due to the absence of polymeric residues after a low temperature curing process.

It is desirable to have the resistivity transition onset temperature, where the resistivity of a silver salt starts changing from a non-conductive state to a conductive state, as low as possible and to have the resistivity transition of a silver salt as rapid as possible. The common belief to date has been that a silver salt with a low thermal decomposition temperature exhibits a resistivity transition behaviour earlier and the final resistivity is the same as long as the molecular fraction of silver is the same. However, here we found that this common belief turned out to be invalid, which is supported by our results that silver 2,2-diethylhexanoate with a lower thermal decomposition curve exhibits a higher resistivity transition behaviour in comparison with silver 2-butylhexanoate, though they are isomeric silver salts, as can be seen in Fig. 3.

Numerous research reports on silver salts are available but they mainly focus on thermal decomposition behaviours,[39,40] structural and phase transitional behaviours,[41] unusual property characterizations,[42,43] and the employment of a silver salt for a final chemical compound,[44] using various analysis techniques such as thermogravimetric analysis (TGA), differential scanning calorimetry (DSC), infrared (IR)/Fourier transform infrared (FTIR) spectroscopy, and X-ray diffraction analysis. The resistivity transition behaviours of silver salts have been presented with their thermal thermograms in some literatures.[19,31,45] However, the discrepancy between the resistivity transition and thermal thermograms of silver salts has not been paid attention and no fundamental resistivity transition mechanism of silver salts has been studied. As a result, the key factors causing the different resistivity transition behaviours of silver salts have remained unanswered to date.

To the best of our knowledge, ink chemists have no decisive criteria to screen silver salts for the selection of the most adequate
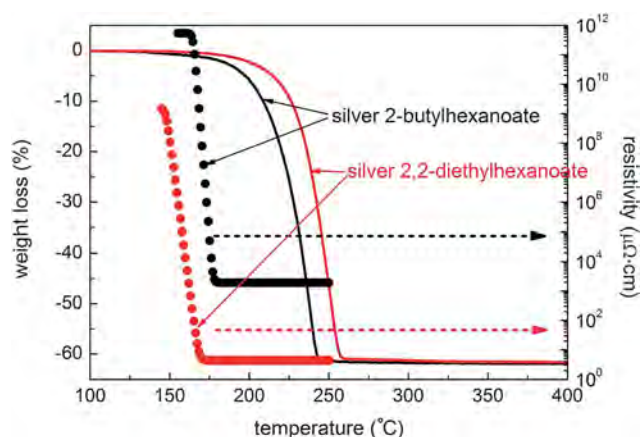
Fig. 3 Inconsistency between TGA thermograms and resistivity transition curves of isomeric silver salts, $C_{10}H_{19}AgO_2$.

one during the formulation of the next generation conductive ink. Therefore, it is quite necessary to be able to identify the key factors of silver salts' resistivity transition. For this fundamental study, we synthesized isomeric silver salts with the same molecular formula, $C_{10}H_{19}AgO_2$, but with different structures because the preparation of a series of isomeric silver salts is crucial for the well-controlled experiments. Then, their electrical properties, morphological traits and thermograms of TGA and DSC were characterized. Here, we newly suggest three major factors, such as stack integrity, phase transition, and the exothermic band in the DSC thermogram, exert a strong influence on the resistivity transition and the final resistivity of isomeric silver salts. Finally, the resulting sheet resistance of a transparent and conductive film with the third generation conductive ink was briefly described when cured at a temperature as low as 150 °C.

2. Experimental

2.1 Synthesis of isomeric silver salts, $C_{10}H_{19}AgO_2$

In this study, the following isomeric silver salts, on the basis of alkanoates with six different structural variants, were synthesized: silver 2-butylhexanoate, silver 2,5-dimethyl-2-ethyl-hexanoate, silver 2-ethyloctanoate, silver 2,2-dimethyloctanoate, silver 2,2-diethylhexanoate, and silver decanoate, as shown in Fig. 4. The detailed synthesis procedures of these isomeric silver salts are described, as follows.

(1) For the silver 2-butylhexanoate, hereinafter referred to as AGS162 ($T_d = 162.3$ °C, where the thermal decomposition onset temperature, T_d, is defined when the mass loss becomes approximately −1 wt%), 2-butylhexanoic acid was prepared from n-hexanoic acid (11.6 g, 0.1 mol) in 12.47 ml of distilled water, and hexyl bromide (16.5 g, 0.1 mol) in 10.8 ml of distilled water (yield 54%). An aqueous equimolar amount of silver nitrate (5.1 g, 0.03 mol) in 200 ml of distilled water was added to 2-butylhexanoic acid (5.2 g, 0.03 mol) in 200 ml of methanol. After stirring for 1 hour at room temperature, the precipitate collected by filtration was washed with distilled water and methanol, followed by drying in a vacuum oven overnight (yield 88%).

(2) For the silver 2,5-dimethyl-2-ethylhexanoate, hereinafter referred to as AGS172 ($T_d = 172.5$ °C), 2,5-dimethyl-2-ethyl-hexanomic acid was prepared from 2-methlybutyric acid (10.2 g,
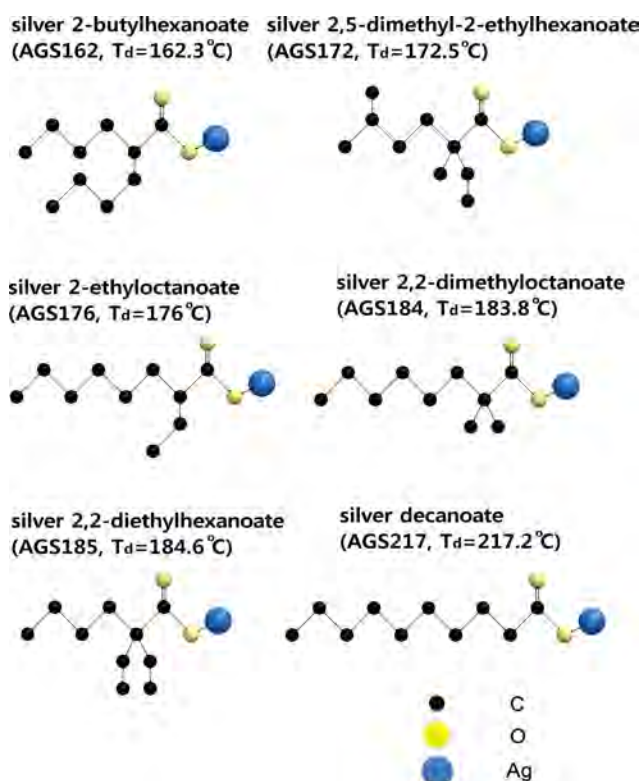

Fig. 4 Structural variants of the synthesized isomeric silver salts, $C_{10}H_{19}AgO_2$.

0.1 mol) and isoamyl bromide (15.1 g, 0.1 mol) (yield 53%). An aqueous equimolar amount of silver nitrate (5.1 g, 0.03 mol) in 200 ml of distilled water was added to 2,5-dimethyl-2-ethyl-hexanoic acid (5.2 g, 0.03 mol) in 200 ml of methanol. The rest of the procedures, from stirring to drying in a vacuum oven, were the same, as described above (yield 87%).

(3) For the silver 2-ethyloctanoate, hereinafter referred to as AGS176 ($T_d = 176$ °C), 2-ethyloctanoic acid was prepared from n-butyric acid (8.8 g, 0.1 mol) in 9.17 ml of distilled water, and hexyl bromide (16.5 g, 0.1 mol) in 14 ml of distilled water (yield 58%). An aqueous equimolar amount of silver nitrate (6.8 g, 0.04 mol) in 200 ml of distilled water was added to 2-ethyl-octanoic acid (6.9 g, 0.04 mol) in 200 ml of methanol. The rest of the procedures, from stirring to drying in a vacuum oven, were the same as above (yield 97%).

(4) For the silver 2,2-dimethyloctanoate, hereinafter referred to as AGS184 ($T_d = 183.8$ °C), 2,2-dimethyloctanoic acid was prepared from isobutyric acid (8.8 g, 0.1 mol) in 9.17 ml of distilled water, and hexyl bromide (16.5 g, 0.1 mol) in 14 ml of distilled water (yield 59%). An aqueous equimolar amount of silver nitrate (9.85 g, 0.058 mol) in 200 ml of distilled water was added to 2,2-dimethyloctanoic acid (10.1 g, 0.058 mol) in 200 ml of methanol. The rest of the procedures, from stirring to drying in a vacuum oven, were the same as above (yield 97%).

(5) For the silver 2,2-diethylhexanoate, hereinafter referred to as AGS185 ($T_d = 184.6$ °C), 2,2-diethylhexanoic acid was prepared from 2-ethylbutyric acid (11.6 g, 0.1 mol) in 12.6 ml of distilled water, and butyl bromide (13.7 g, 0.1 mol) in 10.8 ml of distilled water (yield 49%). An aqueous equimolar amount of silver nitrate (5.1 g, 0.03 mol) in 200 ml of distilled water was

added to 2,2-diethylhexanoic acid (5.2 g, 0.03 mol) in 200 ml of methanol. The rest of the procedures, from stirring to drying in a vacuum oven, were the same as above (yield 82%).

(6) For the silver decanoate, hereinafter referred to as AGS217 (T_d = 217.2 °C), sodium hydroxide (4.0 g, 0.1 mol) in 200 ml of distilled water was added to decanoic acid (17.2 g, 0.1 mol) in 200 ml of methanol and stirred for 1 hour at room temperature. The rest of the procedures, from the addition of an aqueous equimolar amount of silver nitrate (17.0 g, 0.1 mol) to drying in a vacuum oven, were the same as above (yield 90%).

The precipitates thus obtained were analyzed with nuclear magnetic resonance (NMR) spectroscopy (Varian Utility Inova 500 NMR spectrometer, Varian, Inc., USA) using samples with 1 wt% (^{1}H NMR) and 5–10 wt% (^{13}C NMR), IR spectroscopy (FTS 3000, Bio-Rad Laboratories, Inc., USA), an atmospheric pressure chemical ionization mass spectrometer (Finnigan LCQ MS, Thermo Electron Corp., USA), an elemental analyzer (Flash 112 series CHNO analyzer, Thermo Electron Corp., USA) and a thermogravimetric analyzer (TGA/SDTA 851e, Mettler-Toledo AG, Analytical, Switzerland), respectively. The analysis results are summarized in the ESI†.

2.2 Preparation of isomeric silver salt coated specimens and thermal decomposition

The suspensions of isomeric silver salts in xylene at a concentration of approximately 5 wt% were coated with an airbrush (Custom Micron CM-B, Iwata Medea, Inc., USA) on glass substrates heated at 80 °C with a hot plate (RH Digital KT/C, IKA Werke GmbH & Co. KG, Germany) until thick enough films were obtained.

Once the glass substrates had been coated with isomeric silver salts, they were further divided into four pieces, the dimensions of which were around 10 mm by 10 mm, and placed on a hot plate. The hot plate was set at 145, 155, 165, 175, 190, 205, 220, 235 and 250 °C. Its surface temperature was checked and adjusted with a non-contact IR thermometer (Raynger ST, Raytek Corp., USA) within ±3 °C. At each temperature, the isomeric silver salt-coated specimens were cured for 10 min and used for electrical characterization. Another set of specimens for morphological characterization was cured for 5 min at 100, 115, 130, 160, 190 and 220 °C. It is noteworthy that the curing time for the morphological characterization was chosen to be shorter than that for the electrical characterization because a shorter curing time tends to effectively disclose the intermediate thermal decomposition states of isomeric silver salts.

2.3 Characterizations of electrical, morphological and thermal properties

The sheet resistance of the specimens was measured with a four-point probe (Universal probe, Jandel Engineering, Ltd, UK) and a sourcemeter (Model 2400, Keithley Instruments Inc., USA). The maximum sheet resistance, measurable with the sourcemeter, was found to be around 202 MΩ, so that the sheet resistance of the isomeric silver salts—AGS184 cured at 155 °C for 10 min and AGS217 cured at 175 °C for 10 min—was assumed to be 250 MΩ since pseudo-sheet resistance values were required for the Boltzmann approximation later on. The thickness of each
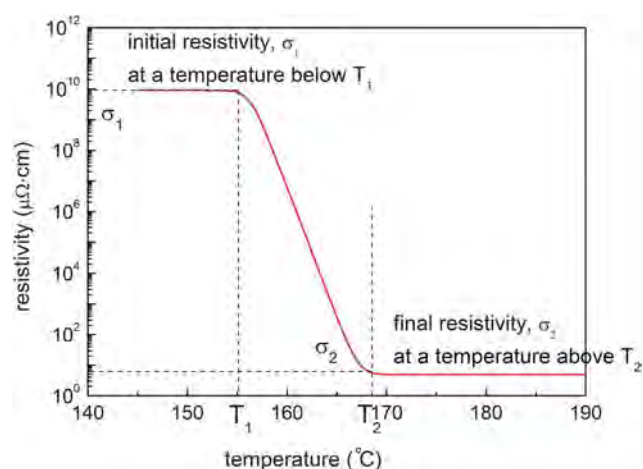

Fig. 5 Sigmoidal resistivity transition of an isomeric silver salt along with the ascending curing temperature.

specimen was measured with a real colour confocal microscope (Optelics C130, Lasertec Corp., Japan).

The resistivity of an isomeric silver salt is postulated to be σ_1 below a certain temperature, T_1, where no isomeric silver salt is decomposed so that it is not conductive, and σ_2 above a certain temperature, T_2, where an isomeric silver salt is fully decomposed so that its resistivity becomes the lowest constant. The resistivity of an isomeric silver salt between T_1 and T_2 can be represented by a sigmoidal curve, as shown in Fig. 5. Once the resistivity of isomeric silver salts at temperatures of 145, 155, 165, 175, 190, 205, 220, 235 and 250 °C was calculated from the measured sheet resistance and thickness, as shown in the ESI†, the Boltzmann approximation with eqn (1) was performed to extract the sigmoidal tendency of the isomeric silver salt's resistivity transition along with the ascending curing temperature, where T, $\sigma(T)$, α and β are temperature, the resistivity function of temperature, and two unknown coefficients, respectively, to be determined with the measured data:

$$\sigma(T) = \frac{\sigma_1 - \sigma_2}{1 + \exp\left(\dfrac{T - \alpha}{\beta}\right)} + \sigma_2 \qquad (1)$$

For the morphological characterization of isomeric silver salts coated onto glass substrates, a low voltage scanning electron microscope (SEM) (S-4800 UHR FE-SEM, Hitachi High-Technologies Corp., Japan) was used. The thermal properties of the isomeric silver salts were re-characterized with a thermal analyzer (Setsys 16/18, SETARAM Instrumentation, France), with which TGA and DSC thermograms were simultaneously measured at a heating rate of 10 °C min^{-1} and a dry air flow rate from 25 to 30 ml min^{-1}.

3. Results and discussion

3.1 Selection of the number of carbon atoms and structure of the hydrocarbon backbone

The basic requirements for a silver salt to produce a good metallic film by thermal decomposition are described in the literature by Vest.[46] Among the ten requirements in the literature,
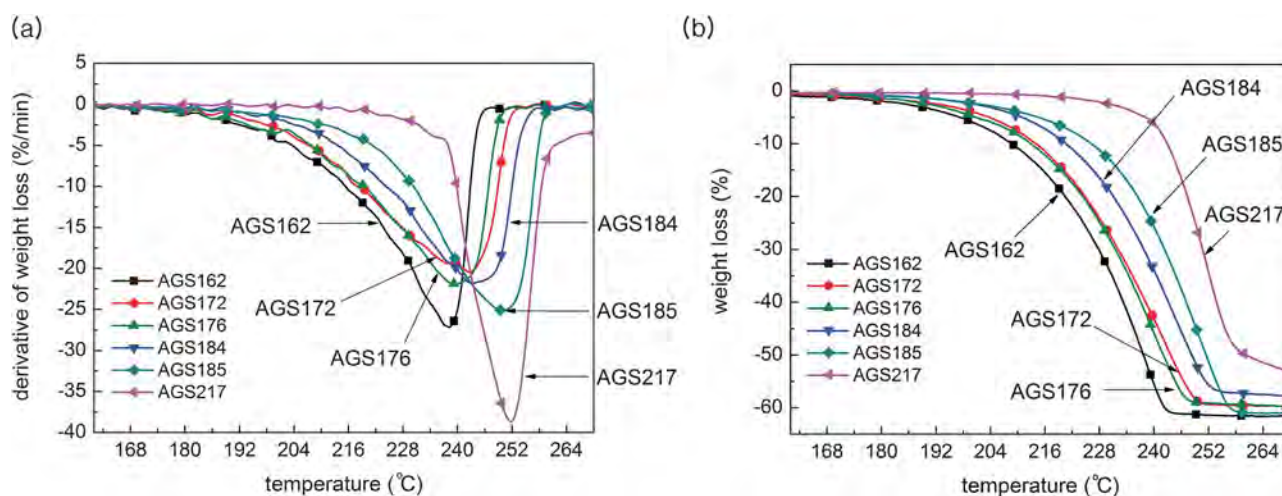
Fig. 6 Thermograms of isomeric silver salts, $C_{10}H_{19}AgO_2$, (a) DTG, and (b) TGA.

two requirements (*i.e.*, high metallic solid content and high solubility in a solvent) are contradictory because the number of carbon atoms should be as small as possible to increase the metallic solid content, but this limits the solubility of the silver salt in a solvent. Therefore, the preferred hydrocarbon backbone and its functional group went to alkanoates such as hexanoate, octanoate and decanoate, where the hydrogen atom is generally substituted with a silver atom. In addition, alkyl groups such as methyl, ethyl and butyl were considered as branches to increase the solubility of an isomeric silver salt in a solvent, when the hydrocarbon backbone was chosen.

Derivative thermogravimetric (DTG) thermograms of synthesized isomeric silver salts were measured and are plotted in Fig. 6(a). Their thermal decomposition temperatures, defined as the temperature where the maximum thermal decomposition rate occurs, were 238.3, 242.8, 239.7, 243.7, 250.1 and 251.8 °C for AS162, AS172, AGS176, AGS184, AGS185 and AGS217, respectively, without any noticeable difference observed within ±6.13 °C. The reason why isomeric silver salts have a similar thermal decomposition temperature is known in the literature that the first fracture in a silver salt during thermal decomposition occurs in the silver–oxygen bond, and this bond breaking temperature is not primarily influenced by the type of hydrocarbon backbone.[45,46] This knowledge leads to the tentative conclusion that the resistivity transition and the final resistivity, σ_2, of isomeric silver salts might be analogous to one another, which contradicts the experimental results of this study. Further detailed experimental results regarding the difference of the resistivity transition and the final resistivity of isomeric silver salts are elucidated hereinafter.

3.2 TGA thermograms and resistivity transition of isomeric silver salts

The colour of the as-deposited isomeric silver salts on the substrate is white or ivory, but as the curing process proceeds, it becomes yellow-brown spot by spot. The origination of the change of colour is controversial because it is inferred to result either from the production of a small amount of Ag_2O owing to the hydrolysis of an isomeric silver salt in humid air, as shown in

eqn (2),[40] or from the production of silver nanoparticles and carbon residues.[41] Irrespective of which mechanism is responsible for the change of colour of an isomeric silver salt, the yellow-brown spots become dark brown as the curing process proceeds. They spread out and eventually cover the entire specimen.

$$2C_nH_{2n+1}COOAg + H_2O \rightarrow Ag_2O + 2C_nH_{2n+1}COOH \quad (2)$$

It is noteworthy that if the curing time is insufficient, the chemical reaction of an isomeric silver salt is not evenly accomplished over the entire area of a specimen, which results in a severe fluctuation of the measured sheet resistance. Therefore, it was decided that the curing time for the electrical characterization of the isomeric silver salts should be 10 min, *i.e.*, two times longer than that for the morphological characterization. If the curing temperature is high enough to fully decompose an isomeric silver salt, the colour of a specimen finally becomes metallic.

The TGA thermograms of isomeric silver salts are shown in Fig. 6(b). As mentioned before, naming of the isomeric silver salts is conducted on the basis of the temperature at which 1 wt% of isomeric silver salts is reduced. Their remaining weight percentages at 510 °C are 38.1, 39.5, 38.0, 40.3, 38.3 and 38.4 wt% for AGS162, AGS172, AGS176, AGS184, AGS185 and AGS217, respectively. These are close to the theoretically predicted one, 38.65 wt%, within an error range running from −1.7 wt% to 0.7 wt%. As postulated in the previous section, the isomeric silver salts are expected to show similar resistivity eventually as their remains show no significant difference and their resistivity transition behaviours must be related to their TGA thermograms, because the TGA thermograms imply the extraction of silver atoms from isomeric silver salts by thermal decomposition.

Fig. 7 shows the measured resistivity data of isomeric silver salts, which are represented by symbols, and the Boltzmann curve fitted lines. The Boltzmann approximation with eqn (1) is found to represent the resistivity transition of the isomeric silver salts fairly well. The ascending order in terms of resistivity transition is AGS176, AGS185, AGS172, AS184, AS162 and AGS217, though one could expect the ascending order to be
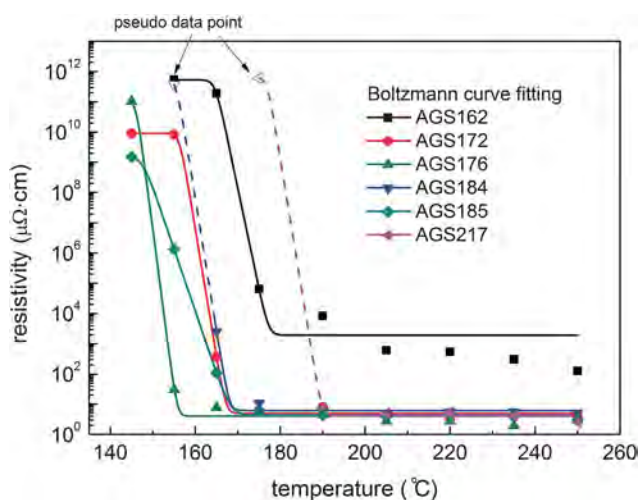
Fig. 7 Resistivity transition curves of isomeric silver salts, $C_{10}H_{19}AgO_2$.

AGS162, AGS172, AGS176, AGS184, AGS185 and AGS217 with the same final resistivity, σ_2, in accordance with the TGA thermograms. Moreover, the final resistivity, σ_2, of AGS162 above 205 °C deviates from that of the other isomeric silver salts. The discordance between the TGA thermograms and the resistivity transition of the isomeric silver salts will be investigated by examining their morphological traits in the next section.

3.3 Influence of morphological stack integrity on final resistivity

The morphological traits of the isomeric silver salts were evaluated by a low voltage SEM, the results of which are shown in Fig. 8, where the isomeric silver salts were cured at 100, 115, 130, 160, 190 and 220 °C for 5 min. Most of the isomeric silver salts were found to exhibit a film-like structure after curing. As can be seen in Fig. 8(e), however, AGS162 differs from the others in the sense that its as-deposited structure remains relatively intact even after curing. In accordance with the initial and final structures of the isomeric silver salts, it is postulated that there are three curing routes for the isomeric silver salts to follow. As can be seen in Fig. 9, a film-like structure after curing is led through curing routes A and A'. The thickness of an as-deposited isomeric silver salt, t_1, is generally reduced to the final thickness, $t_2 < t_1$, due to thermal decomposition. In these cases, the final resistivity, σ_2, of the isomeric silver salts has no significant difference, no matter which initial as-deposited structure they have at room temperature, i.e., either a film-like structure such as AGS176, AGS185, AGS172 and AGS184 or a hay-stacked structure such as AGS217. On the other hand, AGS162 follows another curing route, B, which maintains its as-deposited hay-stacked structure so that the final thickness, t_2, shows a relatively lower reduction from the as-deposited thickness, t_1. However, the resistivity of AGS162 is slightly enhanced as the curing temperature rises due to the fusion of extracted silver nanoclusters by thermal decomposition. This is the reason why the resistivity of AGS162
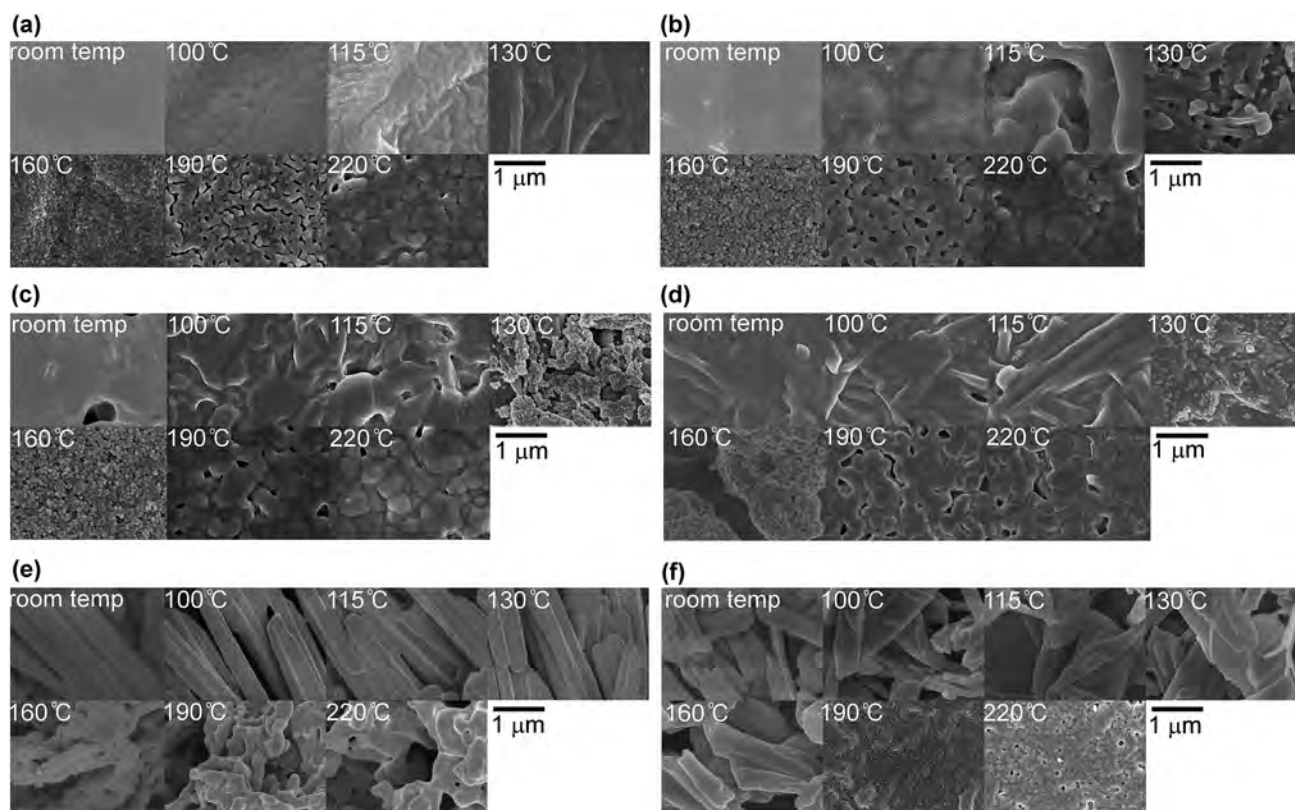

Fig. 8 Morphological transition states of isomeric silver salts from room temperature to 220 °C for 5 min, (a) AGS176, (b) AGS185, (c) AGS172, (d) AGS184, (e) AGS162, and (f) AGS217.

This journal is © The Royal Society of Chemistry 2012

still declined slowly even above 200 °C, as shown in Fig. 7, apart from the Boltzmann approximation.

Up to this point, the cause of the final resistivity difference and the deviation from the Boltzmann approximation is implicated with stack integrity. If the final cured structure is a hay-stacked one, its final resistivity is higher than that of the film-like structure and deviates slightly from the Boltzmann approximation. However, this stack integrity effect does not fully explain why the resistivity transition of isomeric silver salts is not associated with their TGA thermograms. Therefore, the resistivity transition behaviours of isomeric silver salts will be investigated with their DSC thermograms.

3.4 Influence of phase transition of isomeric silver salts on resistivity transition

With the morphological characterization of the isomeric silver salts, the final resistivity difference of AGS162 from the other silver salts is elucidated. However, the cause of the difference in final stack integrity between AGS162 and AGS217, which initially took a very similar hay-stacked structure but resulted in different structures, is not fully understood with the TGA thermograms. For a greater understanding of the final stack integrity difference between AGS162 and AGS217, their heat flow and heat flow rate were characterized and are plotted in Fig. 10.
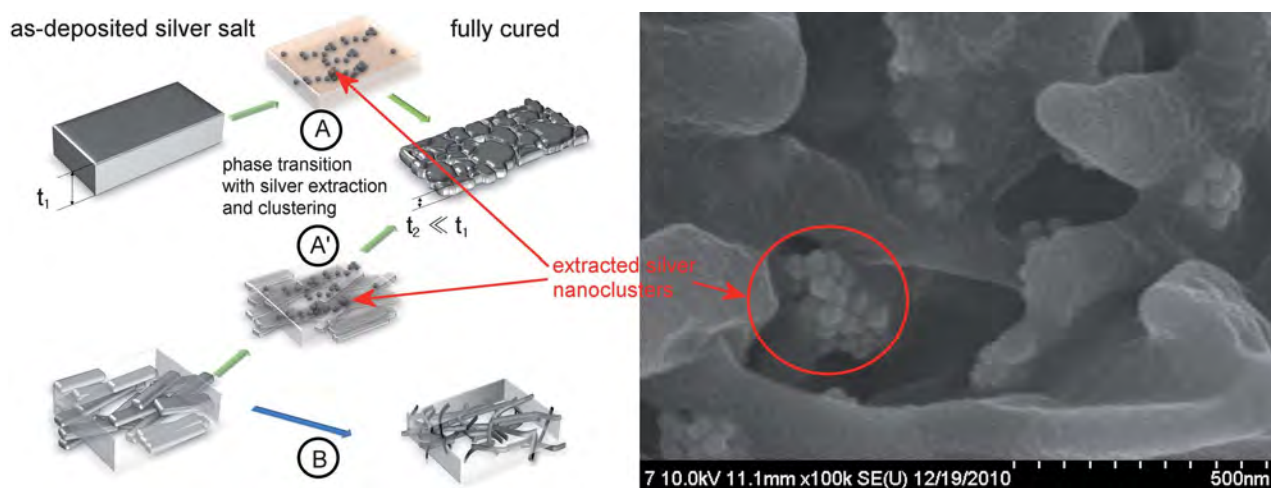

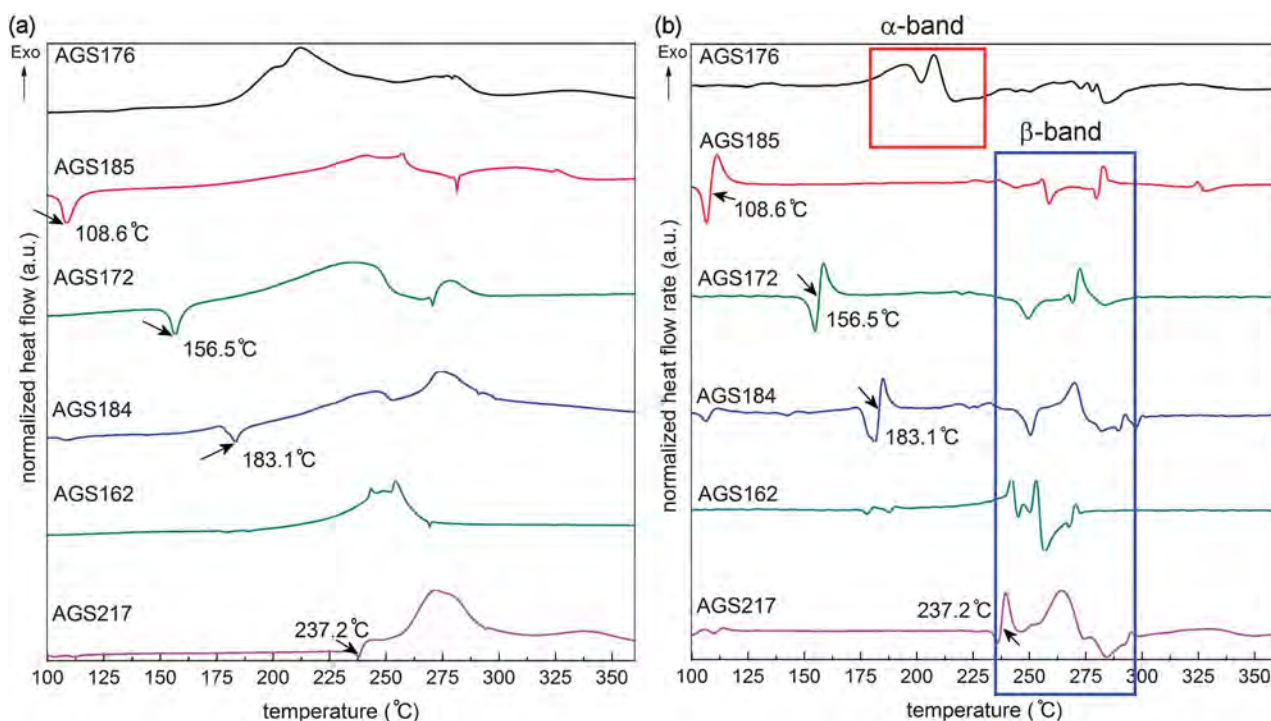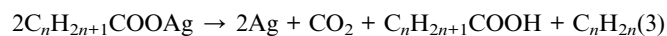**Fig. 9** Resistivity dependency on curing routes, A, A′ and B.

Fig. 10 DSC thermograms of isomeric silver salts and their first derivatives with respect to time, (a) normalized heat flow and (b) normalized heat flow rate.

Where AGS162 and AGS217 are concerned, the noticeable difference between them is the existence of a phase transition peak at 237.2 °C, as indicated with an arrow in Fig. 10(a), in the case of AGS217. If this peak results from the solid-to-liquid phase transition before full thermal decomposition, the lower final resistivity of AGS217 compared to AGS162 is induced by structural collapse due to melting through curing route A′, as shown in Fig. 9.

It is noteworthy that other isomeric silver salts such as AGS185, AGS172 and AGS184 also exhibit strong peaks at 108.6, 156.5 and 183.1 °C, respectively, as shown in Fig. 10(a). Such phase transitions of other silver salts have been reported in numerous literature reports.[41,42,44] They could involve transitions from a crystalline phase to another crystalline phase, from a crystalline phase to a mesophase, from a mesophase to another mesophase, from a mesophase to an amorphous phase, or more complicated multiple transitions in sequence. Although it is not certain whether the peaks shown in Fig. 10 represent either solid-to-solid phase transition or solid-to-liquid phase transition with the TGA/DSC experimental set-up used here, the state of phase transition can be inferred from the decomposition mechanisms of the silver salts, as follows.

$$2C_nH_{2n+1}COOAg \rightarrow 2Ag + CO_2 + C_nH_{2n+1}COOH + C_nH_{2n} \quad (3)$$

$$C_nH_{2n+1}COOAg \rightarrow Ag + CO_2 + C_nH_{2n+1} \quad (4)$$

The by-products of a decomposed isomeric silver salt can be its corresponding alkanoic acid and alkene, no matter which contradicting decomposition mechanisms an isomeric silver salt follows, as shown in eqn (3) (ref. 41) and eqn (4).[47] Where the corresponding alkanoic acids of isomeric silver salts are concerned, their melting temperatures are below 60 °C.[48] When the corresponding alkenes in the form of α-olefins are used as a reference, their melting temperatures are −139.8 °C for 1-hexene, −101.7 °C for 1-octene, and −66.0 °C for 1-decene,[49] though the exact melting temperatures of the corresponding alkenes with branches are unknown. Therefore, those peaks might represent the solid-to-liquid phase transition. In accordance with the visual observation of these isomeric silver salts, however, a wax-like state appeared instead of a complete liquid state during the curing process. This is a similar behaviour to that reported by Binnemans et al.[41] and hence the state of phase transition for AGS185, AGS172 and AGS184 is postulated to be the solid-to-mesophase transition rather than true melting.

Therefore, the resistivity transition of AGS185, AGS172 and AGS184 is postulated to be governed by the solid-to-mesophase transition temperature rather than their TGA thermograms, according to Fig. 7 and 10. Their solid-to-mesophase transition temperatures are also inferred to be influenced by the existence of branches in their hydrocarbon backbones as well as their chain lengths, unlike silver salts such as silver alkanethiolates as seen in the work of Levchenko et al.,[43] which were reported to have no discernible difference of the solid-to-mesophase transition temperatures despite their chain lengths.

Once an isomeric silver salt undergoes the solid-to-mesophase transition, it becomes unstable and hence the silver–oxygen bond breaks easily. As a result, silver nanoclusters are formed even at a temperature lower than its thermal decomposition onset temperature, and the resistivity transition occurs, as shown in the SEM image of Fig. 9. This implies that the lower the solid-to-mesophase transition temperature, the earlier the resistivity transition of an isomeric silver salt will occur.

3.5 Influence of the exothermic band in a DSC thermogram on resistivity transition

Among all the other isomeric silver salts, the resistivity transition of AGS176 deviates from the previously stated explanations with morphological and phase transition characteristics. Very little difference was observed between the TGA thermograms of AGS172 and AGS176. However, the resistivity transition of AGS176 was observed much earlier even without the solid-to-mesophase transition, like AGS185, AGS172 and AGS184. This earlier resistivity transition of AGS176 is postulated to be led by the appearance of the lowest exothermic band in its DSC thermogram, named 'α-band' in Fig. 10(b), compared to 'β-band' from the other silver salts. At this lowest exothermic band, the extraction of silver atom from AGS176 takes place and they form silver nanoclusters. Once silver nanoclusters have formed, they behave as a seed and silver grains grow around them. The monodispersity of the formed silver nanoclusters is known to be influenced by the chain length of the corresponding alkanoic acid, which is adsorbed on the surface of the silver clusters.[40,45,50] These formed silver nanoclusters eventually start forming the conductive network with the adjacent silver nanoclusters and lead to the early resistivity transition.

3.6 Roll-to-roll printed transparent conductive film

The resulting transparent conductive film, which was gravure-offset printed with the next generation conductive ink, is shown in the inset of Fig. 11. The line width and optical transmittance of the gravure-offset printed transparent conductive film were around 20 μm and 85%, respectively, when the line pitch was set at 300 μm. Although the sheet resistance depends on the printed line dimensions such as pitch, width and thickness, the typical
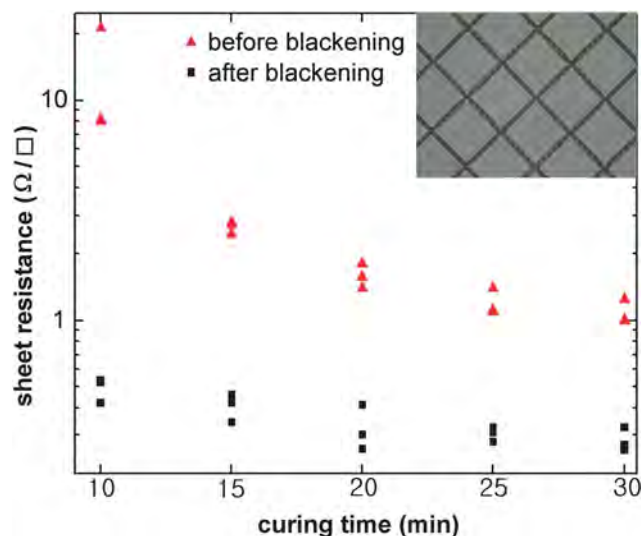

Fig. 11 Sheet resistance of a roll-to-roll printed conductive film, cured at 150 °C.

sheet resistance of the gravure-offset printed one lay in the range from 1 to 30 $\Omega \ \square^{-1}$ when cured at 150 °C. If silver lines were blackened to enhance the contrast ratio of the transparent conductive film, its typical sheet resistance could be as low as 0.3 to 0.4 $\Omega \ \square^{-1}$. It is noteworthy that the inclusion of conductive particles to the solution of a silver salt may affect the formation of the conductive film and further discussions on the effect of conductive particles in combination with a silver salt are found in the work of Chun et al.[31]

4. Conclusions

Unlike the first generation silver salt based ink and the second generation nanoparticle based ink with a polymeric dispersant, the next generation conductive ink for a roll-to-roll printed transparent conductive film contains a silver salt as both a metallic additive and a dispersant. The key to the next generation conductive ink is the selection of a silver salt, which must turn into a metallic state as rapidly as possible at a low curing temperature, and the selection process has been based on the thermogravimetric analysis. Contrary to the common belief, our experimental results show that the TGA thermogram of a silver salt is not coupled with its resistivity transition and final resistivity. To identify the key factors of silver salts' resistivity transition, six different isomeric silver salts, $C_{10}H_{19}AgO_2$, were synthesized in this study and their thermal and electrical properties were characterized, as well as their morphological traits. It was found that the resistivity transition and the final resistivity of the isomeric silver salts are governed by three factors, namely, stack integrity, phase transition, and exothermic band in their DSC thermograms.

Deposited isomeric silver salts have a structure that is either film-like or hay-stacked. If the final structure is a hay-stacked one, its final resistivity is higher than that of a film-like one, though the silver content of the isomeric silver salts is the same. If an isomeric silver salt with a hay-stacked structure undergoes the solid-to-mesophase transition during curing, the final structure becomes a film-like one and no significant difference of its final resistivity is observed.

The resistivity transition of an isomeric silver salt is greatly influenced by the solid-to-mesophase transition. Once an isomeric silver salt experiences the solid-to-mesophase transition, it becomes unstable and hence silver–oxygen bond breaking takes place at a temperature lower than its thermal decomposition onset temperature. The earlier the solid-to-mesophase transition of an isomeric silver salt occurs, the earlier silver nanoclusters are formed. As a result, the resistivity transition of an isomeric silver salt takes place due to the silver nanoclusters embedded in the remains.

Another formidable cause of the earlier resistivity transition is the exothermic band appearing in the DSC thermogram of an isomeric silver salt. Because this exothermic band represents the phenomenal driving source of the thermal decomposition of an isomeric silver salt, the earlier appearance of this band leads to the earlier resistivity transition.

The findings in this study are conducive to the tailoring and selecting of a silver salt for the mixture with solid metal particles in ink as both a metallic additive and a dispersant. By characterizing the DSC thermograms, a suitable silver salt for a low temperature curing process can be identified. Therefore, ink chemists have a new measure to screen synthesized silver salts effectively with a minimal amount, rather than fully formulating conductive inks for a roll-to-roll printed transparent conductive film. This will extend the scope of application of silver salts to not only roll-to-roll printed transparent conductive films but also other printed electronic devices.

Acknowledgements

Notes and references

1 H. Sirringhaus, T. Kawase, R. H. Friend, T. Shimoda, M. Inbasekaran, W. Wu and E. P. Woo, Science, 2000, 290, 2123.
2 S. E. Burns, P. Cain, J. Mills, J. Wang and H. Sirringhaus, MRS Bull., 2003, 28, 829.
3 C. W. Sele, T. von Werne, R. H. Friend and H. Sirringhaus, Adv. Mater., 2005, 17, 997.
4 M. Baklar, P. H. Wöbkenberg, D. Sparrowe, M. Gonçalves, I. McCulloch, M. Heeney, T. Anthopoulos and N. Stingelin, J. Mater. Chem., 2010, 20, 1927.
5 M.-B. Madec, P. J. Smith, A. Malandraki, N. Wang, J. G. Korvink and S. G. Yeates, J. Mater. Chem., 2010, 20, 9155.
6 T. Shimoda, Y. Matsuki, M. Furusawa, T. Aoki, I. Yudasaka, H. Tanaka, H. Iwasawa, D. Wang, M. Miyasaka and Y. Takeuchi, Nature, 2006, 440, 783.
7 D.-H. Lee, S.-Y. Han, G. S. Herman and C. Chang, J. Mater. Chem., 2009, 19, 3135.
8 Y. Liu, T. Cui and K. Varahramyan, Solid-State Electron., 2003, 47, 1543.
9 B. Chen, T. Cui, Y. Liu and K. Varahramyan, Solid-State Electron., 2003, 47, 841.
10 M. Mäntysalo and P. Mansikkamäki, AEU Int. J. Electron. Commun., 2009, 63, 31.
11 M. G. Han, J. Sperry, A. Gupta, C. F. Huebner, S. T. Ingram and S. H. Foulger, J. Mater. Chem., 2007, 17, 1347.
12 J. Perelaer, P. J. Smith, D. Mager, D. Soltman, S. K. Volkman, V. Subramanian, J. G. Korvink and U. S. Schubert, J. Mater. Chem., 2010, 20, 8446.
13 M.-C. Choi, Y. Kim and C.-S. Ha, Prog. Polym. Sci., 2008, 33, 581.
14 M. Wehner, F. Legewie, B. Theisen and E. Beyer, Appl. Surf. Sci., 1996, 106, 406.
15 H. M. Nur, J. H. Song, J. R. G. Evans and M. J. Edirisinghe, J. Mater. Sci.: Mater. Electron., 2002, 13, 213.
16 G. G. Rozenberg, E. Bresler, S. P. Speakman and J. H. G. Steinke, Appl. Phys. Lett., 2002, 81, 5249.
17 D. Li, D. Sutton, A. Burgess, D. Graham and P. D. Calvert, J. Mater. Chem., 2009, 19, 3719.
18 A. L. Dearden, P. J. Smith, D.-Y. Shin, N. Reis, B. Derby and P. O'Brien, Macromol. Rapid Commun., 2005, 26, 315.
19 J. Perelaer, C. E. Hendriks, A. W. M. de Laat and U. S. Schubert, Nanotechnology, 2009, 20, 165303.
20 J. J. P. Valeton, K. Hermans, C. W. M. Bastiaansen, D. J. Broer, J. Perelaer, U. S. Schubert, G. P. Crawford and P. J. Smith, J. Mater. Chem., 2010, 20, 543.
21 S. Magdassi, A. Bassa, Y. Vinetsky and A. Kamyshny, Chem. Mater., 2003, 15, 2208.
22 S. Jang, Y. Seo, J. Choi, T. Kim, J. Cho, S. Kim and D. Kim, Scr. Mater., 2010, 62, 258.
23 P. Buffat and J.-P. Borel, Phys. Rev. A: At., Mol., Opt. Phys., 1976, 13, 2287.
24 W. H. Qi and M. P. Wang, Mater. Chem. Phys., 2004, 88, 280.
25 H.-H. Lee, K.-S. Chou and K.-C. Huang, Nanotechnology, 2005, 16, 2436.

26 J. Perelaer, A. W. M. de Laat, C. E. Hendriks and U. S. Schubert, *J. Mater. Chem.*, 2008, **18**, 3209.
27 M. Grouchko, A. Kamyshny and S. Magdassi, *J. Mater. Chem.*, 2009, **19**, 3057.
28 K. Woo, C. Bae, Y. Jeong, D. Kim and J. Moon, *J. Mater. Chem.*, 2010, **20**, 3877.
29 S. Wolf and C. Feldmann, *J. Mater. Chem.*, 2010, **20**, 7694.
30 D.-Y. Shin, Y. Lee and C. H. Kim, *Thin Solid Films*, 2009, **517**, 6112.
31 S. Chun, D. Grudinin, D. Lee, S.-H. Kim, G.-R. Yi and I. Hwang, *Chem. Mater.*, 2009, **21**, 343.
32 A. Blümel, A. Klu, S. Eder, U. Scherf, E. Moderegger and E. J. W. List, *Org. Electron.*, 2007, **8**, 389.
33 S. H. Ko, H. Pan, C. P. Grigoropoulos, C. K. Luscombe, J. M. J. Fréchet and D. Poulikakos, *Appl. Phys. Lett.*, 2007, **90**, 141103.
34 C. E. Hendriks, P. J. Smith, J. Perelaer, A. M. J. van den Berg and U. S. Schubert, *Adv. Funct. Mater.*, 2008, **18**, 1031.
35 T. Fischer, U. Hahn, M. Dinter, M. Bartzsch, G. Schmidt, H. Kempa and A. C. Huebler, *Org. Electron.*, 2009, **10**, 547.
36 I. M. Krieger, *Adv. Colloid Interface Sci.*, 1972, **3**, 111.
37 J. A. Lewis, *J. Am. Ceram. Soc.*, 2000, **83**, 2341.
38 A. Huebler, U. Hahn, W. Beier, N. Lasch and T. Fischer, Proc. 2 Int. IEEE Conf. Polym. Adhesives Microelectron. Photon., 2002, 172.
39 C.-A. Lu, P. Lin, H.-C. Lin and S.-F. Wang, *Jpn. J. Appl. Phys.*, 2007, **46**, 251.
40 N. F. Uvarov, L. P. Burleva, M. B. Mizen, D. R. Whitcomb and C. Zou, *Solid State Ionics*, 1998, **107**, 31.
41 K. Binnemans, R. van Deun, B. Thijs, I. Vanwelkenhuysen and I. Geuens, *Chem. Mater.*, 2004, **16**, 1021.
42 M. Chadha, M. E. Dunnigan, M. R. V. Sahyun and T. Ishida, *J. Appl. Phys.*, 1998, **84**, 887.
43 A. A. Levchenko, C. K. Yee, A. N. Parikh and A. Navrotsky, *Chem. Mater.*, 2005, **17**, 5428.
44 M. Steffan, A. Jakob, P. Claus and H. Lang, *Catal. Commun.*, 2009, **10**, 437.
45 S. F. Jahn, A. Jakob, T. Blaudeck, P. Schmidt, H. Lang and R. R. Baumann, *Thin Solid Films*, 2010, **518**, 3218.
46 R. W. Vest, in *Ceramic Films and Coatings*, ed. J. B. Wachtman and R. A. Haber, Noyes Publications, Park Ridge, 1993.
47 V. M. Andreev, L. P. Burleva, V. V. Boldyrev and Y. I. Mikhailov, Izv. Sib. Otd. Akad. Nauk USSR Ser. Khim. Nauk, 1983, **4**, 58.
48 ChemSpider, http://www.chemspider.com.
49 Wikipedia, http://www.wikipedia.org.
50 I.-K. Shim, Y. I. Lee, K. J. Lee and J. Joung, *Mater. Chem. Phys.*, 2008, **110**, 316.